Icarus 383 (2022) 115082

Contents lists available at ScienceDirect

Icarus

journal homepage: www.elsevier.com/locate/icarus

Detailed petrogenesis of the unsampled Oceanus Procellarum: The case of the Chang'e-5 mare basalts

Qi He [a,*], Yiheng Li [a], Ioannis Baziotis [b], Yuqi Qian [a], Long Xiao [a,*], Zaicong Wang [a], Wen Zhang [a], Biji Luo [a], Clive R. Neal [c], James M.D. Day [d], Fabin Pan [a], Zhenbing She [e], Xiang Wu [a], Zhaochu Hu [a], Keqing Zong [a], Lu Wang [a]

[a] Planetary Science Institute, State Key Laboratory of Geological Processes and Mineral Resources, School of Earth Sciences, China University of Geosciences, Wuhan 430074, China
[b] Department of Natural Resources Management & Agricultural Engineering, Agricultural University of Athens, Iera Odos 75, Athens 11755, Greece
[c] Department of Civil and Environmental Engineering and Earth Sciences, University of Notre Dame, Notre Dame, IN 46556, USA
[d] Scripps Institution of Oceanography, University of California San Diego, La Jolla, CA 92093-0244, USA
[e] State Key Laboratory of Biogeology and Environmental Geology, China University of Geosciences, Wuhan, China

ARTICLE INFO

Keywords:
Chang'e-5
Young mare basalts
Highly evolved basaltic magma
Oceanus Procellarum
The moon

ABSTRACT

Lunar mare basalts provide a probe to study the magmatic and thermal evolution of the Moon. The Chang'e-5 (CE-5) mission returned samples from a young and hitherto unsampled mare terrain, providing fresh opportunities to understand lunar volcanic history. A detailed petrologic survey was conducted in this study on basalt fragments and glasses from the returned CE-5 soil samples. Relatively large-sized (100–400 μm) basaltic fragments were hand-picked and examined for texture, mineral assemblage and mineral chemistries. Basaltic fragments exhibit dominantly subophitic textures and are phenocryst-free, with low to intermediate-Ti (2.1–5.5 wt%) and low Mg# (Mg/(Mg + Fe) × 100, 19–47, with an average whole-rock Mg# of 33) consistent with olivine-melt equilibrium calculation (Mg# = 34). A range of highly evolved basaltic materials have been identified, in which abundant fayalitic olivine, symplectitic intergrowths, and Si + K-rich mesostasis co-exist were found resulting from late-stage silicate liquid immiscibility. Basaltic glass compositions largely overlap with basaltic fragment compositions suggesting they are locally derived. The CE-5 basalts have a relatively limited range of eruption temperatures of 1150–1230 °C. Based on their petrographic and geochemical characteristics, some CE-5 mare basalts are highly evolved and some of the resultant basaltic melt products underwent high crystallization. Thermodynamic modeling using MELTS suggests highly evolved basaltic magma was produced by a low-pressure and simple fractional crystallization under reduced conditions. This may have occurred at the surface in the inflated Em4/P58 flow with a thickness of ~50 m. The low degree of partial melting mantle source of the parental melts is the late-stage lunar magma ocean cumulates in a similar manner to some evolved low-Ti mare basalt meteorites, although the source of CE-5 basalts may have been slightly more Ti-rich.

1. Introduction

Basaltic mare flows are the dominant volcanic materials on the Moon, covering covering ~17% of the lunar surface (Head III, 1976; Hiesinger et al., 2003), and 18.1% of the lunar surface if cryptomeria are considered (Whitten and Head, 2015). Mare volcanism began after the formation of the Moon, as early as ~4.35 Ga (Apollo 14 basalts, Dasch et al., 1987; Kalahari 009, Terada et al., 2007), and may have ceased at ~1.1 Ga (Hiesinger et al., 2011) or even later (Braden et al., 2014). The driver of the young lunar volcanism is still not clear; possible mechanisms have been proposed include 1) elevated heat-producing elements in the mantle (Ziethe et al., 2009); 2) elevated water abundance in mantle (Saal et al., 2008), or 3) tidal heating (Elkins-Tanton et al., 2011). The Chang'e-5 (CE-5) mission landed in a region of relatively young mare basalts in northern Oceanus Procellarum (1.5–2.0 Ga; e.g., Hiesinger et al., 2011; Qian et al., 2021a) and returned 1731 g of regolith samples. These returned basalts are of great value in understanding the later history of lunar magmatic activity.

* Corresponding authors.
E-mail addresses: he_qi@cug.edu.cn (Q. He), longxiao@cug.edu.cn (L. Xiao).

https://doi.org/10.1016/j.icarus.2022.115082
Received 28 January 2022; Received in revised form 5 May 2022; Accepted 6 May 2022
Available online 11 May 2022
0019-1035/© 2022 Elsevier Inc. All rights reserved.

The CE-5 landing site is close to a large volcanic complex named Mons Rümker (Zhao et al., 2017). Remote observations of the CE-5 landing site and its surroundings show that it is covered by a type of intermediate-Ti mare basalt (TiO_2 in the range of 5 to 8 wt%, FeO of 16.5–17.5 wt%, Th of 5–8.5 ppm, Qian et al., 2021b). Such intermediate-Ti mare basalts are underrepresented in the Apollo and Luna sample collections, due to limited sampling at low latitudes on the lunar nearside (Neal and Taylor, 1992; Giguere et al., 2000). However, the Apollo 12 ilmenite basalts do contain up to 5 wt% TiO_2 (Neal et al., 1994), and Apollo 16 basalt clasts from 60,639 contain 7–8 wt% TiO_2 (Fagan and Neal, 2016). The global TiO_2 map also shows that intermediate-Ti mare basalts are common in the center of the Procellarum KREEP Terrane (Giguere et al., 2000; Jolliff et al., 2000). The bulk composition of the CE-5 basaltic fragments has been estimated to contain intermediate TiO_2 (5.7 wt%) and high FeO (22.2 wt%) (Tian et al., 2021), consistent with the composition of the CE-5 soils (TiO_2 ~ 5.0 wt%; FeO ~22.5 wt%; Li et al., 2022). Additionally, there may be a minor contribution from high-Ti volcanism (Jiang et al., 2021) that was transported to the CE-5 site either through volcanic or impact processes.

Determination of Pb—Pb isochrons for the returned CE-5 basaltic fragments reveal that the Moon was still volcanically active at least 2 billion years ago (Che et al., 2021; Li et al., 2022). However, radiogenic isotope systematics (e.g., Rb—Sr, Sm—Nd and U—Pb), H isotopes, and REE modeling of the returned CE-5 samples collectively indicate that the enrichment of heat-producing elements (Tian et al., 2021) or water (Hu et al., 2021) in the CE-5 mare basalt mantle source regions were not the cause for young lunar volcanism. Therefore, other mechanisms are needed to explain the onset of the young lunar basalts and more detailed sample studies are required to better understand the mantle source region, and the generation, ascent, and eruption of the CE-5 basalts.

Preliminary work has made important advances in the age, petrology and geochemistry of CE-5 samples (Che et al., 2021; Tian et al., 2021; Li et al., 2021; Hu et al., 2021). However, only a few focus on detailed petrological studies (Neal et al., 2022; Webb et al., 2022). These basalts have complex textures, and details regarding the processes responsible for these textures and the evolution of their parental magmas were not reported. Here we studied the low to intermediate Ti and highly evolved CE-5 basaltic fragments, based on petrographic analysis and comparison with Apollo basalts.

2. Sample and methods

The CE-5 scooped sample CE5C0400 (YJFM00403, 200 mg), allocated by the China National Space Administration was used in this study. Approximately 400 soil fragments with grain sizes varying from 100 to 400 μm were hand-picked under a binocular microscope in an ultraclean room environment. About 70 picked regolith fragments were mounted in Araldite 2020 epoxy resin, then polished for petrological studies. All the sample preparation and analysis were conducted at the State Key Laboratory of Geological Processes and Mineral Resources, China University of Geosciences, Wuhan.

The polished mounts were carbon-coated and examined with the scanning electron microscopes (FE-SEM, FEI Quanta 200) equipped with energy dispersive spectrometers (EDS).

Major element compositions of minerals were determined using a JEOL JXA-8230 electron microprobe analyzer (EPMA). Minerals were analyzed using 15 kV accelerating voltage, 20 nA focused beam (1 μm diameter). Plagioclase, phosphate and glasses were analyzed with a slightly defocused beam (5 μm diameter). Natural mineral and glass standards were used with ZAF matrix correction. The standards used were jadeite (Na), olivine (Si), diopside (Ca, Mg), almandine (Fe, Al), sanidine (K), rutile (Ti), rhodonite (Mn), and chromium oxide (Cr). Representative EPMA results are given in Table S1, while the detailed compositions are given in the Tables S2–1 through S2–5.

Major and trace element contents of polymineralic fragments (fine-grained basalts) and basaltic glasses were obtained from the polished mounts using laser ablation inductively coupled plasma mass spectrometry (LA-ICP-MS). Trace element analyses were obtained using an Agilent 7500a ICP-MS coupled with a Geolas 2005 excimer ArF laser (193 nm) ablation system (Lambda Physik, Göttingen, Germany). The repetition rate used was between 6 and 10 Hz. Additionally, incorporating nitrogen into the gas flow helped to increase the detection limit and improve precision (Hu et al., 2008). Each analysis included a background acquisition of 20–30 s (gas blank) followed by 50 s of sample data acquisition. The software ICPMSDataCal was used for off-line selection and integration of the background and analyzed areas, time-drift correction, and data reduction (Liu et al., 2008).

The spot diameter on minerals or glasses was 32 μm. The measured elements were externally calibrated by using multiple USGS glasses (BCR-2G, BHVO-2G, and BIR-1G; preferred values for USGS glasses can be found in Geological and Environmental Reference Materials-GeoReM database http://georem.mpch-mainz.gwdg.de/; Jochum et al., 2005). Between every six unknown sample measurements as least a single measurement of NIST SRM 610 glass was performed in order to standardize sufficiently. Representative major and trace element results using LA-ICP-MS are given in Table S3. More details of standard analyses are given in Table S4.

3. Results

3.1. Crystalline basalts

Crystalline basalts are the dominant lithic fragment in the CE-5 lunar soil sample CE5C0400. A range of textural types within each basalt category represents different cooling histories. The texture of these fragments ranges from poikilitic to porphyritic to sub-ophitic to intersertal (Fig. 1).

Most fragments examined have a sub-ophitic texture. The observed average mineral assemblage (modal content in vol% estimated using ImageJ software; Fig. 1C) is composed of pyroxene (46.7%), plagioclase (41.1%), olivine (8.6%), and ilmenite (2.6%). The composition of the olivine is Fo_{40}; using a K_D value of 0.33 (Grove and Vaniman, 1978) the calculated Mg# of the equilibrium melt is 0.18. Some sub-ophitic basalts are olivine-free and dominated by pyroxene (62.4 vol%), and plagioclase (34.8 vol%) with lesser amounts of ilmenite (2.8 vol%). The pyroxenes have an augitic composition, similar to that measured in Apollo 11 and Apollo 17 basalts. Some pyroxenes are zoned with a compositional range from augite (core) to more Fe-rich rims ($En_{5\text{-}39}Fs_{29\text{-}71}Wo_{24\text{–}32}$) (Fig. S1). The composition of plagioclase is relatively homogeneous ($An_{80\text{–}85}$).

Several basaltic fragments host large olivine (40–150 μm in diameter) or pyroxene (50–100 μm in diameter) grains associated with the earliest stages of crystallization, while a second stage of crystal growth is indicated from microlites (Fig. 1G, H) or dendritic phases (Fig. 1D) of olivine and pyroxene. The larger grains may have crystallized in a subsurface magma chamber and the microcrystals during rapid crystallization after eruption on the lunar surface.

Olivine grains display a bimodal distribution in Fo contents, the larger grains comprising relatively Mg-rich olivine ($Fo_{40\text{–}61}$), and fayalitic olivine (up to Fo_{15}) in the mesostasis (Table S5). The pyroxene compositions show extreme variation in terms of Ca-Mg-Fe contents (Fig. S1). Similar to olivine, the pyroxene grains show normal zoning with extreme Fe-enrichments in their outer portions. Compared to other lunar mare basalts and mare basaltic meteorites, the pyroxene cores are more Fe-rich (Fig. S1). The late-stage Fe-rich pyroxene mainly occurs in and surrounding mesostasis areas, where it approaches pyroxferroite. Plagioclase crystals in all fragments are homogeneous from core to rim within the grains, although the composition changes between different grains ($An_{68\text{–}90}$).

Minor minerals in the basalts include ilmenite, K-feldspar, fayalite, silica (cristobalite, confirmed by Raman), troilite, apatite and merrillite. No Fe-metal grains were found in the fragments, unlike Apollo and Luna

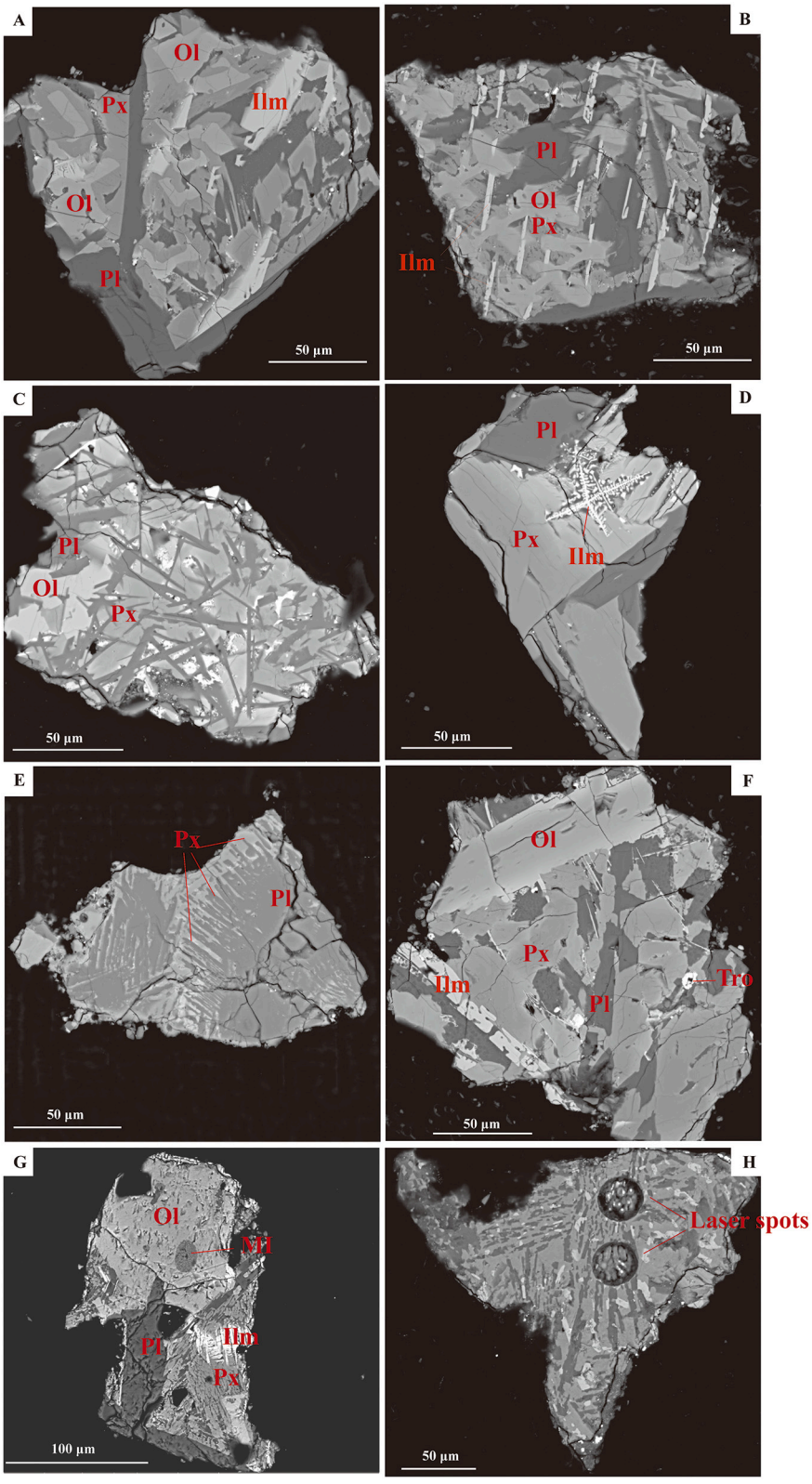

Fig. 1. Representative BSE images of basaltic fragments in CE-5 lunar soil CE5C0400. (A) A basaltic fragment with relatively large crystals; (B) basaltic fragment containing subhedral to anhedral pyroxene and plagioclase, with orientated elongated laths of ilmenite; (C) A relatively fine-grained subophitic textured basaltic fragment. Euhedral plagioclase laths are enclosed by zoned pyroxene and Fe-rich olivine, with minor ilmenite; (D) A basaltic fragment containing zoned pyroxene and euhedral plagioclase, with dendritic ilmenite; (E) acicular texture common to impact melt rocks with fibrous intergrowths of plagioclase and pyroxene microcrystals; (F) porphyritic textured basaltic fragment with large zoned olivine (Ol) with two stages of ilmenite crystallization; the early-stage ilmenite is represented by skeletal crystals, while the second stage by needle shaped; (G) A basaltic fragment with a large olivine phenocryst containing a melt inclusion (MI), and two-stage olivine crystal population with a rapid second stage of crystal growth to form the dendritic phases; (H) A phenocryst-free basaltic fragment, in which the matrix is made of compacted, fine-grained pyroxene, plagioclase and ilmenite. Laser spots used for bulk analysis are visible. Ol = olivine, Px = pyroxene, Ilm = ilmenite, Pl = plagioclase, Tro- troilite, MI-melt inclusion.

mare basalts (Day, 2020). However, the areas covered by these samples is small (Fig. 1) and the absence of Fe metal may be a sampling issue (small sample size). Ilmenite is close to the pure endmember with only trace amounts of other elements including MgO (0.1–1.9 wt%). A few of the Fe—Ti oxides are ulvöspinel, containing Cr_2O_3 in the range of 6.6–12.1 wt%, FeO 55–60 wt%, and TiO_2 25.2–30.7 wt%. Melt inclusions hosted in ilmenite that reported by Hu et al. (2021) were also observed in this study. A few K-rich and Ba-rich feldspars (Table S1; BaO $\leq$ 12.4 wt%, $K_2O \leq$ 8.5 wt%), K-rich glass or silica rich glass included in fayalite occur and are typical late-stage phases. Both merrillite and apatite are present in basaltic fragments. Apatite is the main OH-bearing phase, which is F-rich (3.4–3.6) and Cl-poor (0.2), similar to those from

Hu et al. (2021). Troilite (FeS) occurs as small (<40 μm) irregular grains near or within mesostasis regions.

Among the studied basaltic fragments, eight fine-grain basaltic fragments (phenocryst-free) were chosen for bulk compositional analysis using LA-ICP-MS. These basalts have low to moderate TiO_2 (2.10–5.52 wt%, average = 4.03 wt%), low Al_2O_3 (4.89–13.0 wt%; average = 9.44 wt%), low CaO (10.5–14.0 wt%; average = 12.5 wt%), low MgO (3.37–9.36 wt%; average = 5.75 wt%), high FeO (19.3–25.6 wt%; average = 22.2 wt%), and low Mg# (19–47; average = 33). The compositions are comparable to the respective values obtained from remote spectroscopic estimations (Qian et al., 2021a) and in-situ analyses (Tian et al., 2021).

A range of highly evolved basaltic fragments are found within the lunar soil sample. These fragments (50–150 μm, Fig. 2) are comprised of K- feldspar ($An_{14-21}Ab_{3-4}Or_{76-82}$, Fig. S2), K—Si glass, fayalitic olivine (Fo_{5-15}), evolved hedenbergitic pyroxenes ($Fs_{64}Wo_{34}$; Mg# = 14–20; Fig. 2A) intergrown with the fayalite grains, accessory ilmenite and rare apatite. The mafic minerals are highly ferroan. As the fragments are relatively small it is possible that they originated from a mesostasis portion of a mare basalt. They are so ferroan as to be distinct from Apollo-type KREEP basalts. Some large-grained silica grains (Fig. 2B; 40 μm in diameter) are associated with plagioclase (An_{80}). Some fayalitic olivine have K—Si or Si-rich glass inclusions that show spheroidal textures.

A few fragments also have regions of Si + K-rich mesostasis that may have formed by silicate liquid immiscibility (SLI, Fig. 2F). Such textures have been described by Pernet-Fisher et al. (2014) and Potts et al. (2016) as "sieve" textures and based on the size of the glass droplets, are classified as mature (large glass droplets) or immature (small glass droplets). The mesostasis region in this study displays both mature and immature textures with Si + K rich droplets that have been trapped within host olivine grains (Fig. 2F). More details of mesostaisis regions are shown in Fig. 3. The texture of these regions implies these basaltic fragments have undergone SLI splitting into Si-K-rich and Fe-rich conjugate liquids (Pernet-Fisher et al., 2014). The mesostasis boundaries can be diffuse (Fig. 3B and D). The modal proportion of fayalite relative to K—Si glass within these mesostasis regions can also vary (Fig. 3). The globules of K-rich glass are both fine-grained and coarse-grained and irregular in morphology. All these textures are consistent with the low Mg# mesostasis pockets described by Roedder and Weiblen (1970, 1971, 1972) and Pernet-Fisher et al. (2014), implying the late-stage residual liquids are relatively low-Mg#.

3.2. Basaltic glasses

Glassy material (excluding agglutinates) in CE-5 lunar soil can be divided into two main categories: 1) spherical glass beads, which are highly variable in color, as described in Li et al., 2022; 2) irregularly shaped glass fragments with shell-like fractures (Fig. S2). A glass particle with a horn-like shape (Fig. S2c) was also found. In our study, the grain size of the glass varies from ~300 μm down to 50 μm.

The irregularly shaped glasses are homogenous and have basaltic compositions, although different glass have compositional variations. The glass LS-209 is designated as low-TiO_2 glass, with TiO_2 ~ 1.6 wt%, SiO_2 48.2 wt%, and Mg# 50. The other glasses display a wide range of compositions, with TiO_2 4.9–6.3 wt%, SiO_2 44.5–48.3 wt%, and relatively uniform Mg# (29.4–31.2; Table S2).

To understand the origin of these homogeneous glasses, typical geochemical criteria (i.e., MgO/Al_2O_3 and CaO/Al_2O_3) were used to classify rock types (see Fig. 4; Delano, 1986; Naney et al., 1976; Zeigler et al., 2006). They are characterized by low MgO/Al_2O_3 (<1.25), high CaO/Al_2O_3 (>0.75) ratios and plot outside the "pyroclastic glasses" field. We therefore define them as "basaltic glasses" (Zeigler et al., 2006; Zeng et al., 2020), consistent with glasses derived from impacts into the local basalts in the vicinity of the CE-5 landing site (Qian et al., 2021c). The basaltic glasses plot in the region of the low MgO/Al_2O_3 (0.5–0.9) and low CaO/Al_2O_3 (0.9 to 1.1) population of basaltic fragments reported from this study (Fig. 4), and the average composition of the CE-5 lunar soil given in Li et al. (2022).

The chondrite-normalized REE patterns of the basaltic glasses show that they are LREE-enriched, with $(La/Sm)_N$ of 1.24–1.61 and a $(La/Yb)_N$ of 1.59–2.04 (Fig. 5). The basaltic fragments are slightly enriched in the REE compared with the Apollo low-Ti basalts and even the highly evolved La Paz basaltic meteorites (e.g., Day et al., 2006a), but have lower REE concentrations than most KREEP basalts. The average basaltic fragments have REE concentrations almost identical to the basaltic glasses, implying their close relation. Trace element compositions of basaltic fragments and glasses in the CE-5 lunar soil show different Mg#, Rb/Th, K/Th, from Apollo low-Ti basalts, KREEP basalts, which may reflect their mantle reservoirs and formation conditions were also different from that of Apollo low-Ti and KREEP basalts (Fig. 6).

4. Discussion

4.1. Parent melt compositions

Based on the basaltic fragments, all appear to be low to intermediate-Ti (TiO_2 2.1–5.5 wt%), with low K_2O (up to 0.21 wt%) average bulk contents, according to the classification scheme of Neal and Taylor (1992). Most of the mare basalts from the Apollo and Luna collections have Mg# higher than 35 (Shearer and Papike, 1993; Shearer et al., 2006). Based on the new mare basalt type proposed by Fagan and Neal (2016), compositionally the CE-5 basaltic fragments are most akin to Apollo 12 low-K basalts (Neal and Taylor, 1992).

The Mg# of the parent melt ($Mg\#_{melt}$) for a given basalt can be predicted from the forsterite of liquidus olivine phases (Ol_{Fo}), assuming that these were in equilibrium with the melt when they formed. To do this, the following equation is used (Roeder and Emslie, 1970; Niu et al., 2002).

$$Mg\#_{melt} = 1/([1/Ol_{Fo} - 1]/K_d + 1)$$

where K_d is the distribution coefficient describing the exchange of Fe and Mg between olivine and a coexisting basaltic melt. For lunar low-Ti melts this distribution coefficient has been determined to be 0.33 at low pressures (Grove and Vaniman, 1978; Longhi et al., 1978). By taking the most forsteritic olivine compositions ($Fo_{0.61}$; sample #133 in CE5C0400) as an estimate of olivine composition, the melt Mg# for the basalts is 0.34. The calculated $Mg\#_{melt}$ is similar to the average Mg# of the basaltic fragments (0.33), therefore, the average bulk compositions of all these fine grain basaltic fragments are interpreted as being likely representative of their parent melts from which they crystallized.

Olivine is among the earliest crystallizing phases in lunar mare basalts. Based on the method described in Papike et al. (1999), we estimated the distribution of Co and Ni between the most Mg-rich olivine cores and the melt:

$$D_{Ni} = (124.13/MgO_{Melt}) - 0.897$$

$$D_{Co} = 0.235 \times D_{Ni} + 0.476$$

where D is the cation ratio of Ni and Co, between olivine and melt. The calculated D_{Ni} (using MgO_{Melt} 6 wt%) and D_{Co} are 19.8, and 5.13, respectively.

Using the most Mg-rich olivine composition (Co = 97 ppm, Ni = 123 ppm), the calculated melt composition for Co = 19 ppm and for Ni = 6 ppm. This result is close to the low Co and Ni in basaltic fragments. Therefore, it can be inferred that the olivine in the samples is in equilibrium with the basaltic fragments (free of phenocrysts), and so reflect an original melt composition. Therefore, the overall bulk compositions of the CE-5 basalts strongly implicate closed-system fractional crystallization after emplacement.

The composition of basaltic glasses is consistent with that of basalt

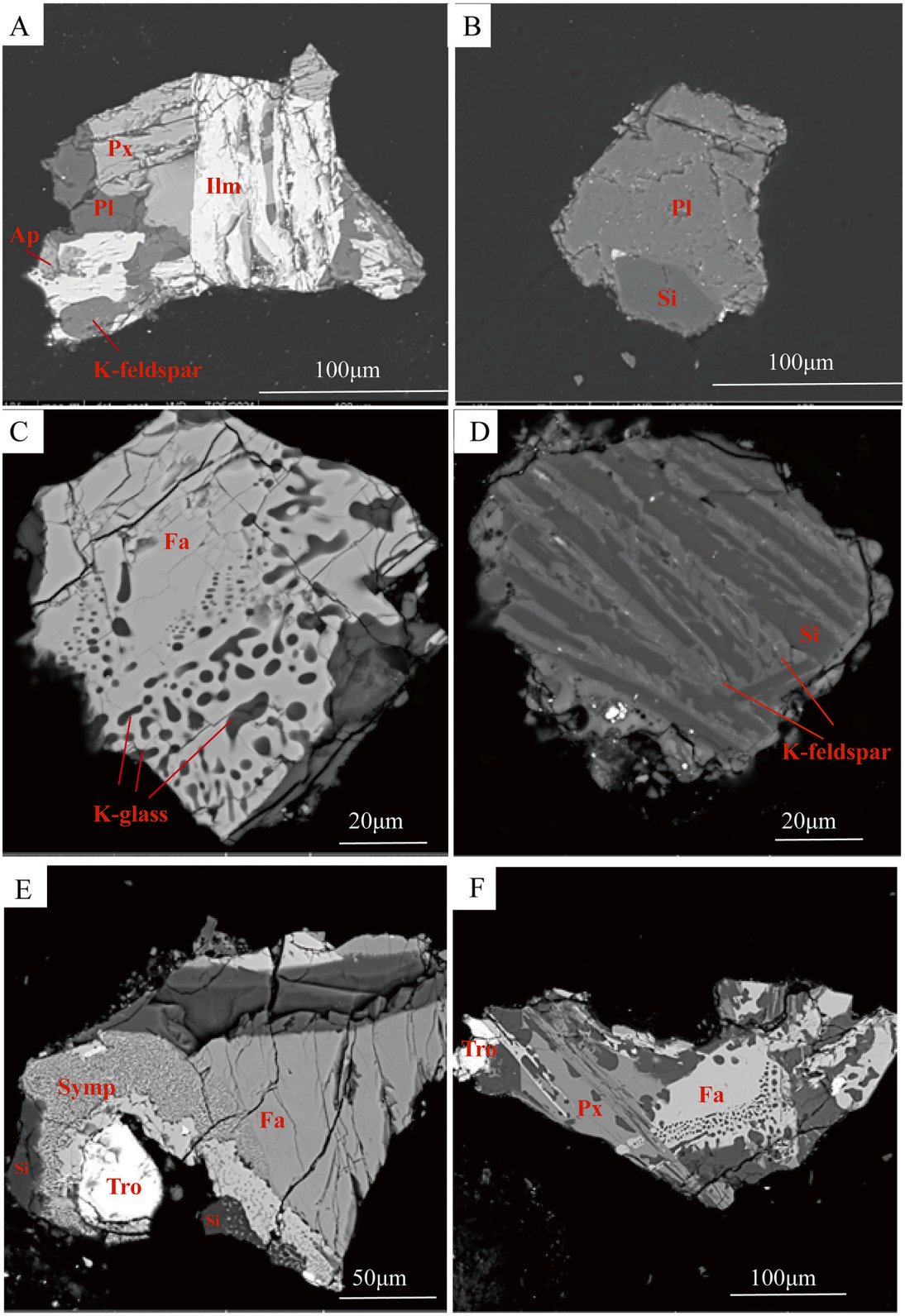

Fig. 2. Back scatter electron (BSE) images of the highly evolved basaltic fragments. (A) A possibly highly evolved mare basalt fragment. The basaltic fragment consists of pyroxene (Mg# = 19.9), plagioclase ($An_{61.7}$) and ilmenite with a few K-feldspars ($An_{14\text{-}21}Ab_{3\text{–}4}Or_{76\text{–}80}$), apatite and Fe-rich olivine ($Fo_{10.3}$). (B) A plagioclase associate with a large silica phase (97 wt% SiO_2). (C) A fayalitic olivine which has K—Si or silica glass inclusions. (D) Intergrowths of K-feldspar with silica that could represent a mesostasis assemblage in a mare basalt. (E) A basaltic fragment contains a high proportion of symplectite that consists of ferro-augite, fayalite, and a silica phase. In the symplectite, the bright phase is fayalite, grey is ferro-augite, and dark grey is silica. Troilite exists juxtaposed to the symplectite. (F) A basaltic fragment with regions of Si + K-rich mesostasis that may have formed by silicate liquid immiscibility. Phase abbreviations: Py, pyroxene; Pl, plagioclase; Tro, troilite; Symp, symplectite; Fa, fayalite; Si, Silica; Ilm, ilmenite; Ap, apatite.

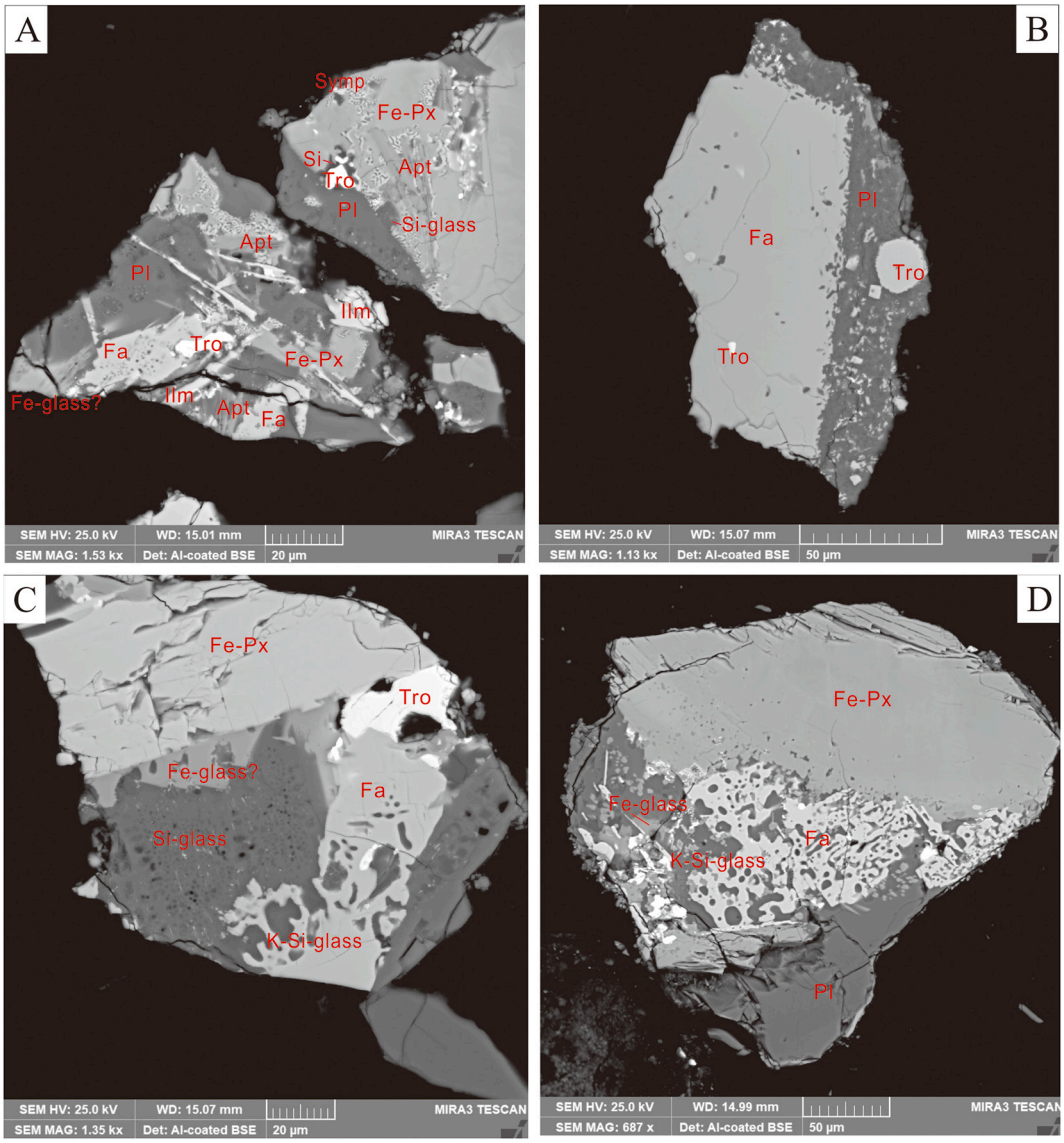

Fig. 3. Back scatter electron (BSE) images of basaltic fragments with regions of Fa (fayalite) and Si + K-rich mesostasis that may have formed by silicate liquid immiscibility. Phase abbreviations: Py, pyroxene; Pl, plagioclase; Tro, troilite; Symp, symplectite; Fa, fayalite; Si, Silica; Ilm, ilmenite; Apt, apatite.

fragments, indicating these basaltic glasses are formed by impact-melting of local basalts. The low-Ti basaltic glass (LS-209) is the only possible exception to this rule, having high MgO (9.5 wt%) and Mg# (0.50) compared with the other basaltic glasses. The incompatible trace element concentrations are slightly lower than other basaltic glasses (Fig. 4), but similar to the basaltic fragments reported by Tian et al. (2021) and Li et al. (2021). Consequently, basaltic glass LS-209 may represent an original and primitive composition to all the other CE-5 mare basalts.

4.2. Magma evolution

4.2.1. Petrographic and REE constraints

From a petrological perspective, large numbers of highly evolved fragments present in CE-5 material suggests that they may be important evidence for significant basaltic magma evolution, all the way to Fe and Si late-stage silicate liquid immiscibility (SLI). Typical mare basalts undergo silicate liquid immiscibility (SLI) at ≥85% crystallization (Roedder and Weiblen, 1970; Rutherford et al., 1974; Pernet-Fisher et al., 2014). However, the petrologic experiments suggest that the Apollo sample 12,032,366–18 (Th-rich) start SLI at ~80% crystallization and began at 1030 °C and 1002 °C (Stadermann et al., 2022). These experiments yielded similar petrographic textures to the fragments identified in this study exhibiting evidence of SLI (Figs. 2 and 3). Therefore, the CE-5 basalts might have also undergone at least 80% crystallization to reach the observed late-stage SLI (similar to the SLI texture in Apollo basalts; Roedder and Weiblen, 1971, 1972), although in detail the composition of the CE-5 basalts and 12,032 are distinct.

Hess et al. (1975) concluded that the fractionation path required for ultimate immiscibility of the residual is similar to the "Fenner trend" (i.e., concentration of Fe into the residual without significant silica enrichment). As concluded above, the parental melt of the CE-5 basalts was relatively enriched in Fe (i.e., Mg# of 0.34), so it is possible that the immiscibility gap would have been reached at lower degrees of fractional crystallization (e.g., Roedder, 1978).

Trace element and REE profiles for CE-5 basaltic fragments and basaltic glasses show similarities to those of the youngest basaltic meteorites, Northwest Africa (NWA) 032, NWA 4734, LaPaz Icefield (LAP) 02205, although the incompatible trace elements concentrations are higher in the CE-5 basaltic fragments and glasses (Fig. 5 and Fig. S3). Northwest Africa 032, NWA 4734, LAP 02205 and the olivine gabbro lithology in NWA 773(2.9–3.1 Ga, Borg et al., 2009; Shaulis et al., 2017),

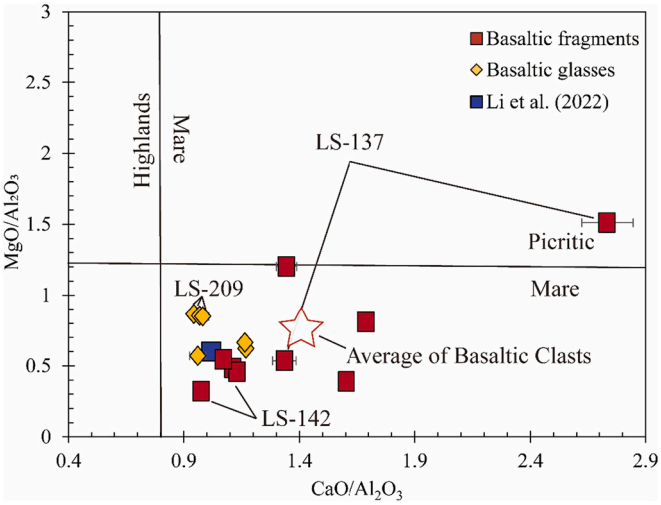

Fig. 4. CaO/Al_2O_3 versus MgO/Al_2O_3 for basaltic glasses and basaltic fragments. Horizontal line (i.e., $MgO/Al_2O_3 = 1.25$) distinguishes pyroclastic from impact mare glass (Delano, 1986). The vertical line (i.e., $CaO/Al_2O_3 = 0.75$) distinguishes highland impact glasses from mare impact glasses (Naney et al., 1976; Zeng et al., 2020). The blue square corresponds to the average bulk-chemical composition of the CE-5 lunar soil measured using X-Ray Fluorescence (Li et al. (2022). (For interpretation of the references to color in this figure legend, the reader is referred to the web version of this article.)

are relatively rich in Fe and incompatible trace elements compared with other low-Ti basalts collected during the Apollo missions (e.g., Day et al., 2006a, 2006b; Elardo et al., 2014). The CE-5 basalts have relatively lower Mg#, and higher trace element enrichment (about 140 times La_N) compared with the LaPaz mare basalts but lower than KREEP, distinguishing them from this latter basalt type (Warren, 1988; Papike et al., 1998).

Previous study of the LAP meteorites has shown that the REE pattern of a 1% partial melt of cumulates formed between 86 and 95% lunar magma ocean (LMO) solidification (Elardo et al., 2014, using the Snyder Model of LMO crystallization and assuming 1% trapped instantaneous residual liquid) has a $(La/Yb)_N$ of 1.48, a $(La/Sm)_N$ of 1.08, and a Eu/Eu* of 0.50. These REE concentrations are similar to the CE-5 basaltic fragments and basaltic glasses. From these observations, we suggest that the CE-5 basalts also derived from relatively low degree partial melting of a relatively late-stage lunar cumulate mantle source.

When comparing the CE-5 basalts with the Th-rich sample 12,032,366,38, their bulk compositions are similar to each other for most of the major and trace element concentrations (Fig. S4, Stadermann et al., 2022, FeO = 19.5 wt%, TiO_2 = 4.22 wt%, Al_2O_3 = 11.7 wt%, MgO = 7.2 wt% for 12,032, 366). Apollo 12,032,366,38 may represent a basalt from western Oceanus Procellarum, owing to its Th-rich composition (7 ppm) and young age, perhaps delivered to the Apollo 12 site by an impact occurring sometime 500–700 m.y. ago (Barra et al., 2006). The CE-5 basalts and Apollo sample 12,032,366 also show similar textures, mineral chemistry, and mesostasis regions. It is possible that 12,032, 366 may represent a rock from the same (or similar) magma chamber from which CE-5 basalts originated.

4.2.2. Temperature and pressure conditions of CE-5 basalt crystallization

The temperature in a basaltic system can be calculated using the whole rock MgO content using the following equation: T (in °C) = 26.3 × MgO + 994.4 (Putirka, 2008). Using this approach, the average MgO content (5.75 wt%) estimated for the CE-5 basaltic fragments equates to a temperature of about 1150 °C. Similarly, the average calculated eruption temperature for the CE-5 basalts using the methods of Jones (2003) is 1153 °C [$T = 948.5 + 48.59 \times MgO - 2.771 \times (MgO)^2 + 0.0882 \times (MgO)^3$].

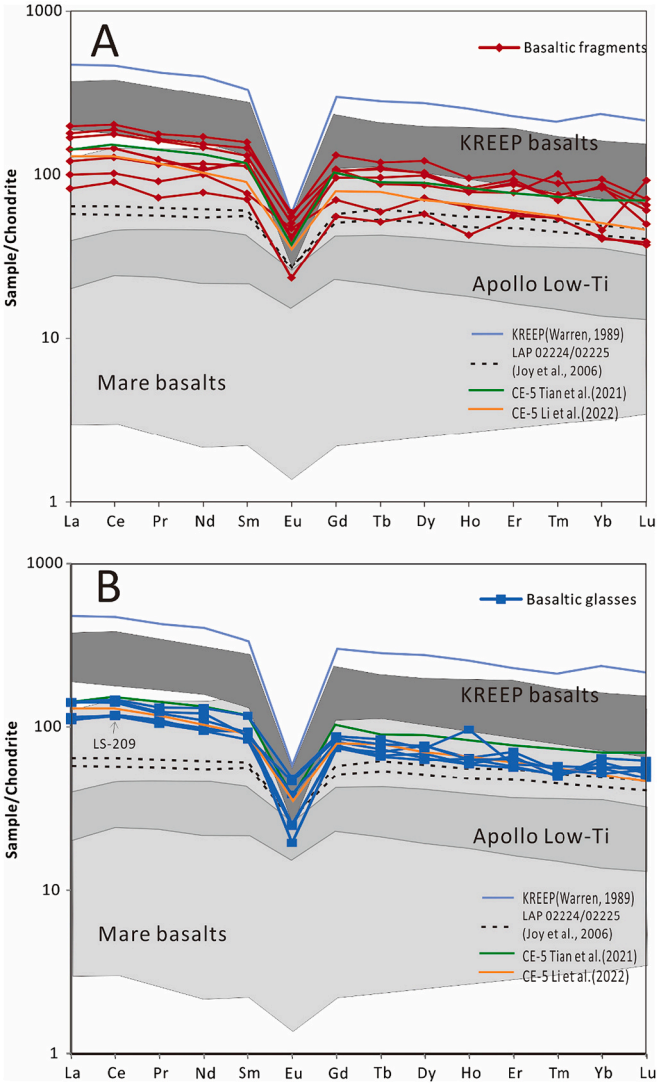

Fig. 5. Basaltic fragments and basaltic glasses REE abundances normalized to CI chondrite (Sun and McDonough, 1989) compared with the melt clasts and KREEP clast within SaU 169 meteorite (dark grey field, Gnos et al., 2004) and high-K KREEP (Warren, 1989). Chondrite normalized bulk REE composition compared with Apollo low-Ti mare basalts (light grey field), and with young evolved low-Ti lunar meteorite LAP 02205/02224 (Joy et al., 2006). All Apollo compositions and fields are from Wieczorek et al. (2006) and Joy et al. (2011).

From the chemical compositions of pyroxene, the crystallization temperatures have been estimated to range from 1200 to 1000 °C for the cores and below 800 °C for the rims (Tian et al., 2021). If the high MgO basaltic glass (LS-209) is an original melt composition, then the eruption T is about 1230 °C. Therefore, the eruption temperature estimated for CE-5 basalts should be around 1150–1230 °C, which appears to be slightly lower to those of the less-evolved Apollo 12 and Apollo 15 low-Ti basalts (1150–1350 °C; Papike et al., 1998).

To investigate the pre-eruption pressure for the CE-5 basalts, both the geochemical characteristics and also the mineral chemistry have to be considered. Experimental study shows the Fe- and incompatible trace element-rich basaltic lunar meteorites LAP 02205, NWA 032, and NWA 4734 have a multiple saturation point at a relatively high liquidus pressure of <0.6 GPa (<105 km) (Elardo et al., 2015). Based on similarities in composition, CE-5 basalts likely had similar pressure conditions to the LAP, NWA 032, and NWA 4734 meteorites. For CE-5 basalts, some extreme Fe-rich pyroxenes have similar compositions to that of pyroxferroite (Fig. S1). The pyroxenes have compositions within the

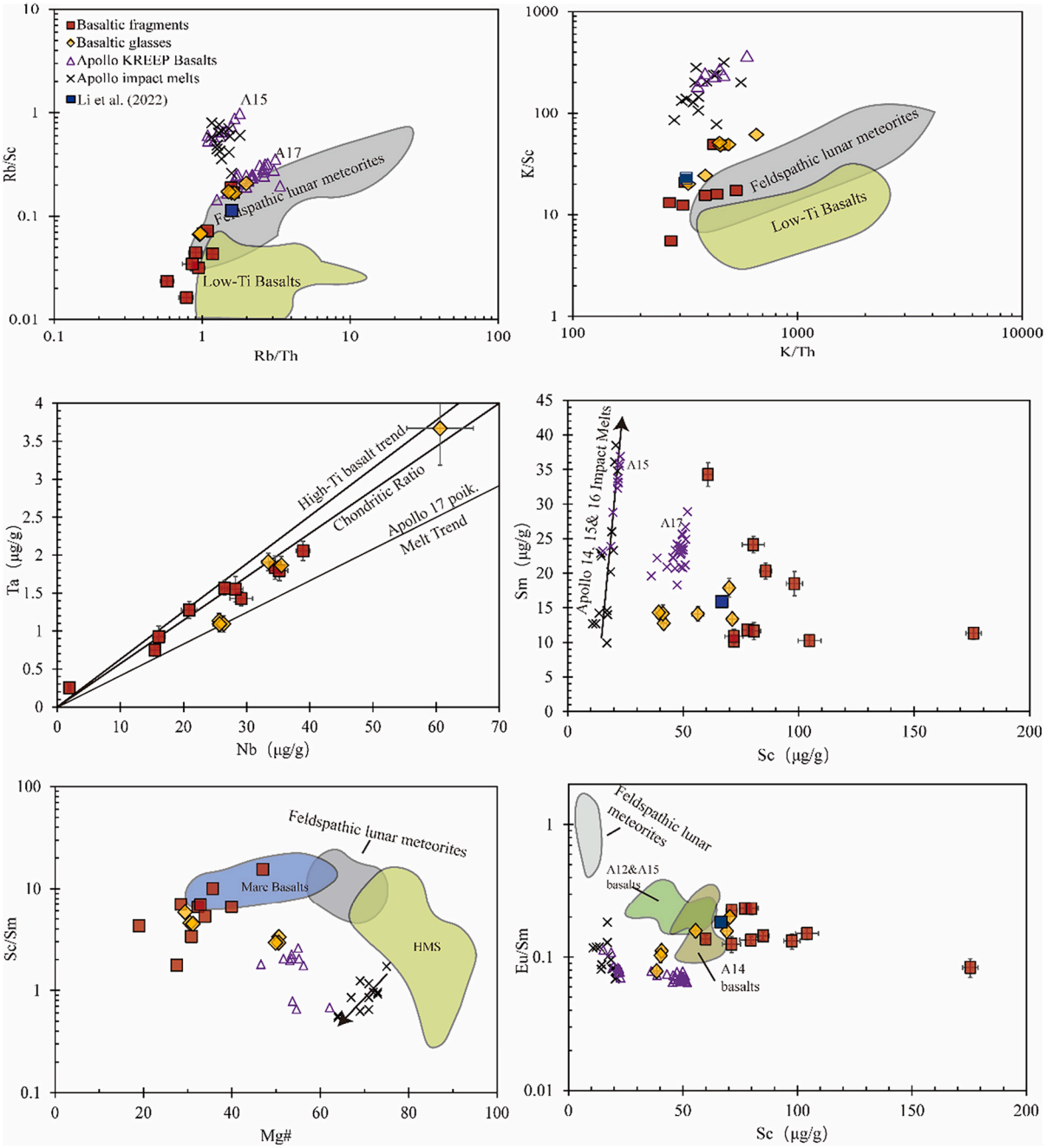

Fig. 6. Trace element compositions of basaltic fragments and glasses in the CE-5 soil compared with Apollo samples (Wieczorek et al., 2006; Joy et al., 2011), Apollo impact melts (Jolliff, 1998), high-K KREEP (Warren, 1989), feldspathic lunar meteorites ('Lunar Meteorite Compendium' resource and references therein) (a) Rb/Th (ppm) versus Rb/Sc (ppm). (b) K/Th (ppm) versus K/Sc (ppm). (c) Nb (ppm) versus Ta (ppm) where Apollo trend lines for the high-Ti basalts, chondritic values (low-Ti mare basalts) and Apollo 17 poikilitic melt trends are taken from Fig. 3.14 of Shearer et al. (2006). (d) Sc (ppm) versus Sm (ppm). (e) Mg# versus Sc/Sm. (f) Sc versus Eu/Sm (ppm).Black solid line errors represent the 1σ analytical errors. The grey dashed errors represent the 1 SD of fragment heterogeneity for fragments where numerous data points were collected (impact melt and low-Ti basalt fragments). Grey A15 symbol = Apollo 15 KREEP basalts. Grey A17 symbol = Apollo 17 KREEP basalts. HAS = High Alkali Suite. HMS = High Magnesium Suite.

forbidden zone, suggesting that the basalts have undergone very rapid cooling (Lindsley, 1983). Lindsley and Burnham (1970) demonstrated that the presence of pyroxenoid in lunar basalts indicates metastable crystallization near or on the lunar surface. Late-stage symplectite consisting of ferro-augite, fayalite, and a silica phase also occurred in several fragments (Fig. 2), which is the break-down product of pyroxferroite. For most pyroxenes in CE-5 basalts, the crystallization pressure can be calculated at between 0.1 MPa to 0.5GPa (Fig. S1).

4.2.3. *Crystallization process modeling*

The easyMelts software (ver. 0.2) –a user-friendly engine for MELTS– was used to track the behavior of major elements in CE-5 (Ghiorso and Sack, 1995; Asimow and Ghiorso, 1998; Asimow, 1999; Ghiorso et al., 2002; Asimow et al., 2001, 2004; Smith and Asimow, 2005). We used the sample LS-64-1 as the starting composition (the most primitive basaltic fragment in our dataset with highest MgO content) and assessed if its liquid line of descent passes through the more evolved compositions. We have examined isobaric crystallization at various pressures

(we present here only the 1 bar, and 5 kbar cases), and fO_2 conditions at 1 °C steps. For the fO_2 we choose reduced conditions at iron-wustite (IW) or just below it (Haloda et al., 2009; Day, 2020; Schwinger and Breuer, 2022).

The 1 bar model predicts olivine as the liquidus mineral at ~1216 °C, followed by pigeonite, low-Ca pyroxene (at ~1156 °C), clinopyroxene (at ~1147 °C), plagioclase (at ~1125 °C), and spinel (at ~1102 °C). The predicted olivine range starts at Fo_{67} (first liquidus phase) and proceeds down to almost pure fayalitic at temperatures as low as ~1025 °C. The observed olivine composition matches the predicted at the temperature range between 1182 °C (Fo_{62}) and 1112 °C (Fo_{40}). Further, the observed pyroxene lies within the predicted range as given in Fig. 7A. In contrast, the MELTS calculations for the high-pressure case (at 5 kbar) can be precluded as suggested by the mismatch of the mineral sequence (early phase clinopyroxene followed by spinel, plagioclase, and then olivine), and modeled olivine compositions with the observed ones. Our preferred case is the one calculated at low-pressure, as expressed by both the curves at 1 bar and 1 kbar (Fig. 8A). Furthermore, in the MgO versus SiO_2 diagram, the 1 bar model fits well the observed data (Fig. 8). There is a discrepancy in fitting the 1 bar model in MgO versus TiO_2 space, however, which may be related to the choice of TiO_2 content in the starting melt. Similarly, the low-pressure models (1 bar and 1 kbar) fit well to the observed Al_2O_3 sample data, except two limited samples (at 4.89 wt% and 12.98 wt% Al_2O_3). Our results are consistent with previous estimates for other lunar basalts (e.g., LAP 02205, LAP 02224, LAP 02226, LAP 02436 and LAP 03632) in which a low-pressure fractional crystallization is the prevalent scenario (Righter et al., 2005). Furthermore, the analyzed pyroxenes show a decrease in the Ti/(Ti + Cr) ratio with increasing Mg# (Fig. S1C) suggesting normal basaltic fractionation (Joy et al., 2006; Day et al., 2006a). Additionally, the Ti versus Al relation reflects a progressive switch from Fe-poor to Fe-rich pyroxenes (Fig. S1D); even though the Mg-rich compositions (pigeonite) are lacking from CE-5 basalts, it seems that the crystallization process is similar to that which occurred for the Apollo 12 and 15 basalts but, in the case of the CE-5 basalts, from more Fe-rich primary melts (Bence and Papike, 1972; Day et al., 2006a). Consequently, the observed pyroxene data are in accordance with the proposed –single fractionation model– derived from this study. Despite possible complications (modifying pressure, oxygen fugacity, starting composition, mixed crystallization scenario-starting with equilibrium and followed by fractional crystallization)

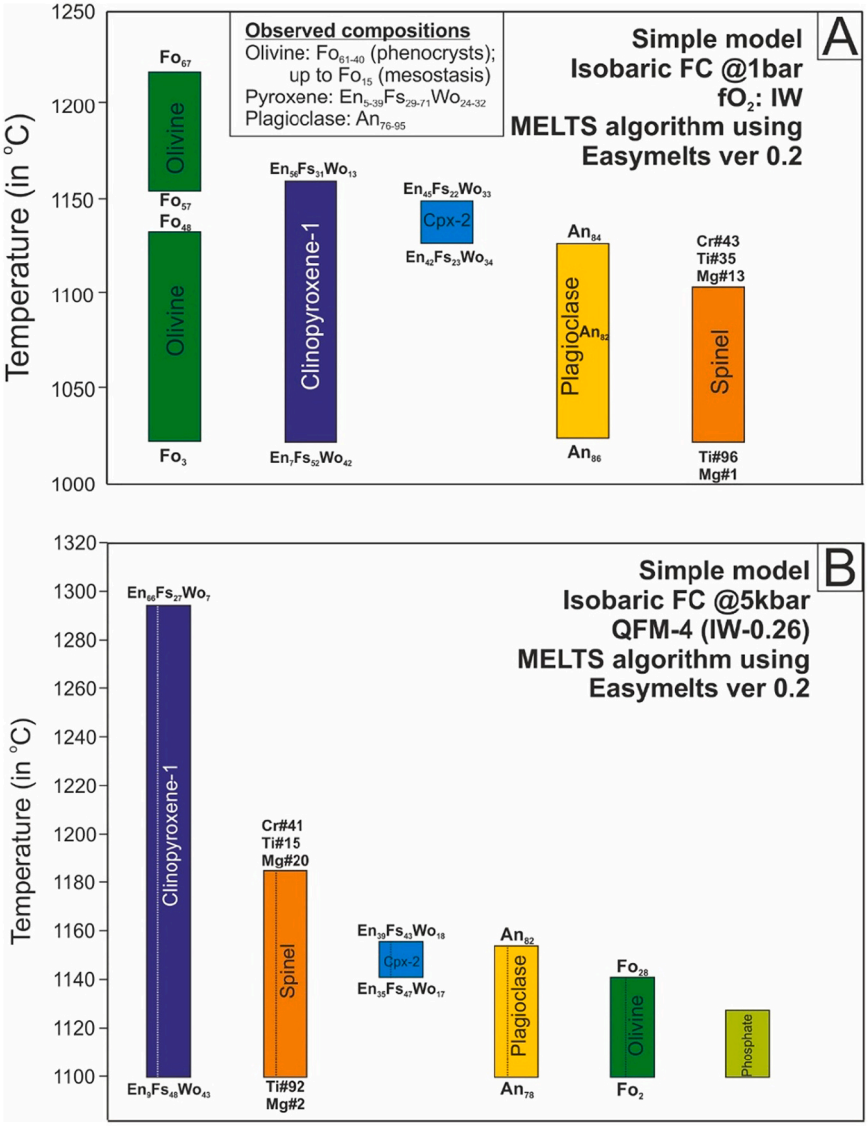

Fig. 7. MELTS modeling using easyMelts (ver. 0.2) algorithm for the less fractionated –basaltic fragment– composition (sample 64–1). Various cases have been tried (assuming different primary melt, fO_2, starting pressure), but here only the a near Fe-FeO fO_2 calculation for (A) pressure 1 bar and (B) pressure 5 kbar are presented. Further, the modeled compositions are compared with the observed ranges.

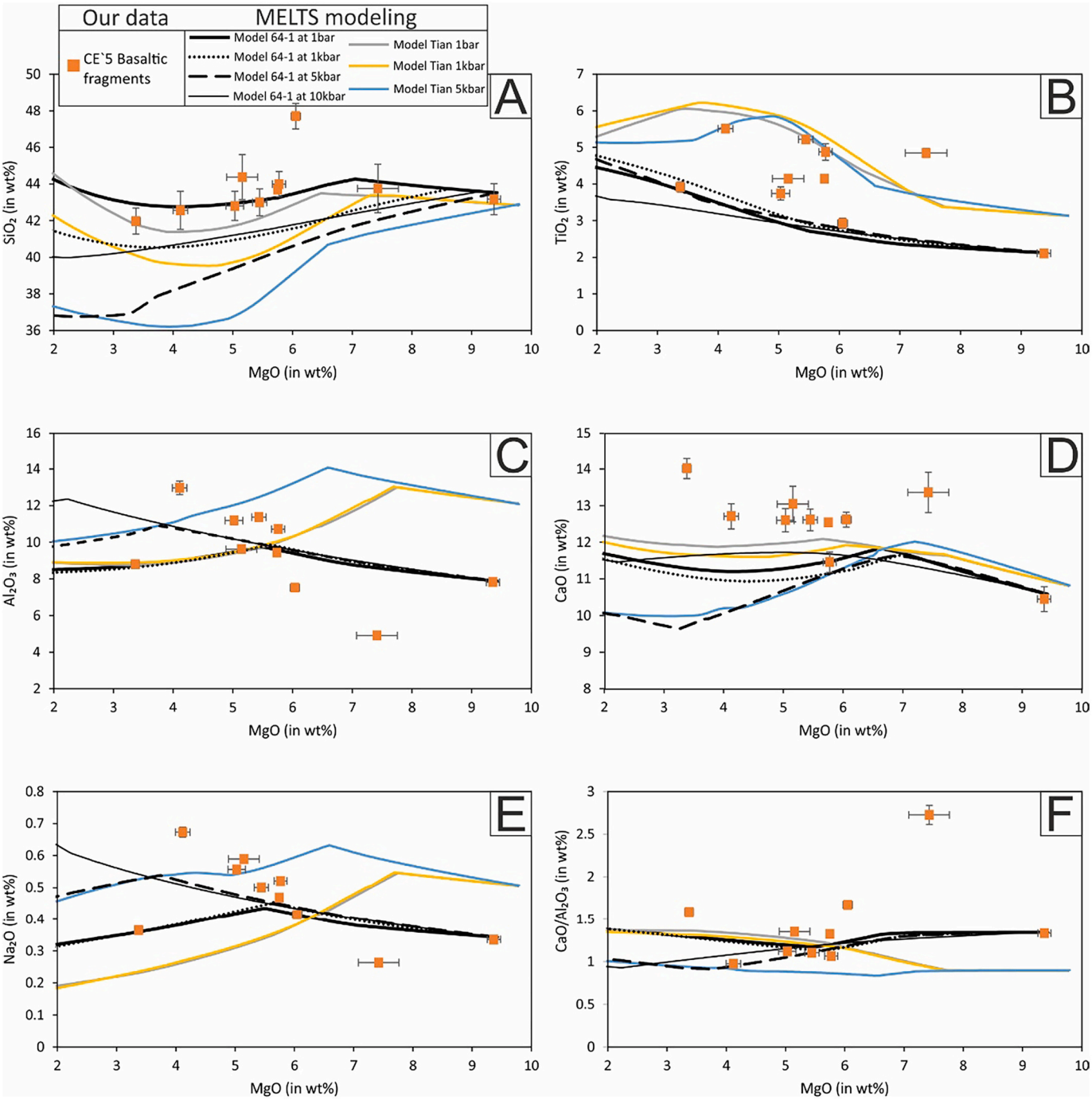

Fig. 8. MgO variation diagrams for (A) SiO_2, (B) TiO_2, (C) Al_2O_3, (D) CaO, (E) Na_2O, and (F) CaO/Al_2O_3. MELTS modeling is depicted as curves calculated at reduced (fO_2 = IW), and isobaric (1 bar, 1 kbar, 5 kbar, and 10 kbar) condition, with two different starting melt compositions (sample 64–1 from this study, and fragment 042GP,002 in table 5 of Tian et al., 2021).

potentially associated with the crystallization of these basalts, this simplified low-pressure model fits more fully than any other scenario that we examined.

4.2.4. *Crystallization environment of the CE-5 basalts*

Wilson et al. (2022) modeled the emplacement of the large volume ~ 270 km long Em4/P58 lava flow, the products of which were sampled by the CE-5 mission. They noted that the lava flowed to the north and ponded around the vent before flowing south to pond again in a depression between Mons Rümker and the Marian crater (Qian et al., 2021c). It was then inflated to its current 50 m thickness (Qian et al., 2021c). Differentiation of this 50 m-thick inflated flow is possible given that radiative cooling formed a crust ~0.47 m thick (Wilson et al., 2022) and cooling would have been slowed due to the input of hot magma near its base during the inflation process. Such cooling would have facilitated the extreme differentiation products as contained in the CE-5 samples and described here.

5. Conclusions

The CE-5 basaltic fragments acquired from the young lunar mare terrain in northern Oceanus Procellarum show a sequence of textural

types, including sub-ophitic and phenocryst-free. The bulk compositions of these basaltic fragments show that they are low-Ti, low MgO and high FeO, with an average Mg# = 0.33. Consequently, these basaltic fragments also confirm the presence of low to intermediate-Ti, high FeO basalts in the Em4/P58 region.

The homogeneous glasses have similar composition to the basaltic fragments and were derived from impact melting of local basaltic material. A few fragments show highly evolved characteristics with assemblages of fayalitic olivine, quartz, and regions of Si + K-rich mesostasis that may have formed by silicate liquid immiscibility (SLI). Based on comparisons with previous experimental studies, it is concluded that the CE-5 basalts underwent ~80% crystallization prior to SLI formation, although the Fe-rich parent melt (Mg# of 0.34) may have meant that the immiscibility gap may have been reached at low degrees of crystallization.

The REE patterns of basaltic fragments and glasses have relatively high REE concentrations when compared with young lunar meteorites (NWA 032, LAP and NWA 4734), but lower than those observed in Apollo KREEP basalts. CE-5 basalts likely derive from relatively low degrees of partial melting of a late-stage cumulate lunar mantle source, similar to some lunar mare basalt meteorites (NWA 032, LAP and NWA 4734).

The eruption temperature estimated for CE-5 basalts was between 1150 °C and 1230 °C. A simplified low-pressure model fits better than other possible scenarios we examined. Our results imply that the CE-5 basaltic fragments formed by low-pressure crystallization of a low-degree partial melt. The observed crystallization is likely to have occurred during the slow cooling of the inflated Em4/P58 flow, which attained a thickness of 50 m (Qian et al., 2021c; Wilson et al., 2022).

Declaration of Competing Interest

None.

Acknowledgments

We thank China National Space Administration (CNSA) for supporting the Chang'e-5 mission and providing access to the CE-5 sample CE5C0400. This research is funded by the Pre-Research Project on Civil Aerospace Technologies funded by CNSA (D020205, D020101). Many thanks also go to the colleagues in the State Key Laboratory of Geological Processes and Mineral Resources, China University of Geosciences, Wuhan for providing technical support. We extend our sincere gratitude to editor Dr. Doris Breuer and two reviewers Dr. Joshua Snape and Dr. Ananya Mallik for their assistance in improving the manuscript.

Appendix A. Supplementary data

Supplementary data to this article can be found online at https://doi.org/10.1016/j.icarus.2022.115082.

References

Asimow, P.D., 1999. A model that reconciles major-and trace-element data from abyssal peridotites. Earth Planet. Sci. Lett. 169 (3–4), 303–319.
Asimow, P.D., Ghiorso, M.S., 1998. Algorithmic modifications extending MELTS to calculate subsolidus phase relations. Am. Mineral. 83 (9–10), 1127–1132.
Asimow, P.D., Hirschmann, M.M., Stolper, E.M., 2001. Calculation of peridotite partial melting from thermodynamic models of minerals and melts, IV. Adiabatic decompression and the composition and mean properties of mid-ocean ridge basalts. J. Petrol. 42 (5), 963–998.
Asimow, P.D., Dixon, J.E., Langmuir, C.H., 2004. A hydrous melting and fractionation model for mid-ocean ridge basalts: application to the mid-Atlantic ridge near the Azores. Geochem. Geophys. Geosyst. 5 (1).
Barra, F., Swindle, T.D., Korotev, R.L., Jolliff, B.L., Zeigler, R.A., Olson, E., 2006. $^{40}Ar/^{39}Ar$ dating of Apollo 12 regolith: implications for the age of Copernicus and the source of nonmare materials. Geochim. Cosmochim. Acta 70 (24), 6016–6031.
Bence, A.E., Papike, J.J., 1972. Pyroxenes as recorders of lunar basalt petrogenesis: chemical trends due to crystal-liquid interaction. In: Lunar and Planetary Science Conference Proceedings, vol. 3, pp. 431–469.
Borg, L.E., Gaffney, A.M., Shearer, C.K., DePaolo, D.J., Hutcheon, I.D., Owens, T.L., Brennecka, G., 2009. Mechanisms for incompatible-element enrichment on the moon deduced from the lunar basaltic meteorite Northwest Africa 032. Geochim. Cosmochim. Acta 73 (13), 3963–3980.
Braden, S.E., Stopar, J.D., Robinson, M.S., Lawrence, S.J., van der Bogert, C.H., Hiesinger, H., 2014. Evidence for basaltic volcanism on the moon within the past 100 million years. Nat. Geosci. 7, 787–791.
Che, X., Nemchin, A., Liu, D., Long, T., Wang, C., Norman, M.D., Webb, S.G., 2021. Age and composition of young basalts on the moon, measured from samples returned by Chang'e-5. Science 374 (6569), 887–890.
Dasch, E.J., Shih, C.-Y., Bansal, B.M., Wiesmann, H., Nyquist, L.E., 1987. Isotopic analysis of basaltic fragments from lunar breccia 14321 chronology and petrogenesis of pre-Imbrium mare volcanism. Geochim. Cosmochim. Acta 51, 3241–3254.
Day, J.M.D., 2020. Metal grains in lunar rocks as indicators of igneous and impact processes. Meteorit. Planet. Sci. 55 (8), 1793–1807.
Day, J.M.D., Taylor, L.A., Floss, C., Patchen, A.D., Schnare, D.W., Pearson, D.G., 2006a. Comparative petrology, geochemistry, and petrogenesis of evolved, low-Ti lunar mare basalt meteorites from the LaPaz icefield, Antarctica. Geochim. Cosmochim. Acta 70 (6), 1581–1600.
Day, J.M.D., Floss, C., Taylor, L.A., Anand, M., Patchen, A.D., 2006b. Evolved mare basalt magmatism, high mg/Fe feldspathic crust, chondritic impactors, and the petrogenesis of Antarctic lunar breccia meteorites Meteorite Hills 01210 and Pecora escarpment 02007. Geochim. Cosmochim. Acta 70 (24), 5957–5989.
Delano, J.W., 1986. Pristine lunar glasses: Criteria, data, and implications. J. Geophys. Res. Solid Earth 91 (B4), 201–213.
Elardo, S.M., Shearer, C.K., Fagan, A.L., Borg, L.E., Gaffney, A.M., Burger, P.V., Neal, C. R., Fernandes, V.A., McCubbin, F.M., 2014. The origin of young mare basalts inferred from lunar meteorites Northwest Africa 4734, 032, and LaPaz icefield 02205. Meteorit. Planet. Sci. 49 (2), 261–291.
Elardo, S.M., Shearer, C.K., Vander Kaaden, K.E., McCubbin, F.M., Bell, A.S., 2015. Petrogenesis of primitive and evolved basalts in a cooling moon: experimental constraints from the youngest known lunar magmas. Earth Planet. Sci. Lett. 422, 126–137.
Elkins-Tanton, L.T., Burgess, S., Yin, Q.Z., 2011. The lunar magma ocean: reconciling the solidification process with lunar petrology and geochronology. Earth Planet. Sci. Lett. 304 (3–4), 326–336.
Fagan, A.L., Neal, C.R., 2016. A new lunar high-Ti basalt type defined from clasts in Apollo 16 breccia 60639. Geochim. Cosmochim. Acta 173, 352–372.
Ghiorso, M.S., Sack, R.O., 1995. Chemical mass transfer in magmatic processes IV. A revised and internally consistent thermodynamic model for the interpolation and extrapolation of liquid-solid equilibria in magmatic systems at elevated temperatures and pressures. Contrib. Mineral. Petrol. 119 (2), 197–212.
Ghiorso, M.S., Hirschmann, M.M., Reiners, P.W., Kress, V.C., 2002. The pMELTS: a revision of MELTS for improved calculation of phase relations and major element partitioning related to partial melting of the mantle to 3 Gpa. Geochem. Geophys. Geosyst. 3 (5), 1–35.
Giguere, T.A., Taylor, G.J., Hawke, B.R., Lucey, P.G., 2000. The titanium contents of lunar mare basalts. Meteorit. Planet. Sci. 35 (1), 193–200.
Gnos, E., Hofmann, B.A., Al-Kathiri, A., Lorenzetti, S., Eugster, O., Whitehouse, M.J., Greenwood, R.C., 2004. Pinpointing the source of a lunar meteorite: implications for the evolution of the moon. Science 305 (5684), 657–659.
Grove, T.L., Vaniman, D.T., 1978. Experimental petrology of very low TI/VLT/basalts. In: Mare Crisium: The View from Luna 24, pp. 445–471.
Haloda, J., Týcová, P., Korotev, R.L., Fernandes, V.A., Burgess, R., Thöni, M., Košler, J., 2009. Petrology, geochemistry, and age of low-Ti mare-basalt meteorite Northeast Africa 003-A: a possible member of the Apollo 15 mare basaltic suite. Geochim. Cosmochim. Acta 73 (11), 3450–3470.
Head III, J.W., 1976. Lunar volcanism in space and time. Rev. Geophys. 14, 265–300.
Hess, P.C., Rutherford, M.J., Guillemette, R.N., Ryerson, F.J., Tuchfeld, H.A., 1975. Residual products of fractional crystallization of lunar magmas: an experimental study. Proc. Lunar Sci. Conf. 6th, 895–909.
Hiesinger, H., Head III, J.W., Wolf, U., Jaumann, R., Neukum, G., 2003. Ages and stratigraphy of mare basalts in Oceanus Procellarum, Mare Nubium, Mare Cognitum, and Mare Insularum. J. Geophys. Res. 108 (E7), 5065. https://doi.org/10.1029/2002JE001985.
Hiesinger, H., Head, J.W., Wolf, U., Jaumann, R., Neukum, G., 2011. Ages and stratigraphy of lunar mare basalts: a synthesis. Geol. Soc. Am. Spec. Pap. 477, 1–51.
Hu, Z., Gao, S., Liu, Y., Hu, S., Chen, H., Yuan, H., 2008. Signal enhancement in laser ablation ICP-MS by addition of nitrogen in the central channel gas. J. Anal. Atomic Spec. 23 (8), 1093–1101.
Hu, S., He, H., Ji, J., Lin, Y., Hui, H., Anand, M., Ouyang, Z., 2021. A dry lunar mantle reservoir for young mare basalts of Chang'E-5. Nature 1–8.
Jiang, Y., Li, Y., Liao, S., Yin, Z., Hsu, W., 2021. Mineral chemistry and 3D tomography of a Chang' E 5 high-Ti basalt: implication for the lunar thermal evolution history. Sci. Bull. https://doi.org/10.1016/j.scib.2021.12.006.
Jochum, K.P., Nohl, U., Herwig, K., Lammel, E., Stoll, B., Hofmann, A.W., 2005. GeoReM: a new geochemical database for reference materials and isotopic standards. Geostand. Geoanal. Res. 29 (3), 333–338.
Jolliff, B.L., 1998. Large-scale separation of K-frac and REEP-frac in the source regions of Apollo impact-melt breccias, and a revised estimate of the KREEP composition. Int. Geol. Rev. 40 (10), 916–935.
Jolliff, B.L., Gillis, J.J., Haskin, L.A., Korotev, R.L., Wieczorek, M.A., 2000. Major lunar crustal terranes: surface expressions and crust-mantle origins. J. Geophys. Res. Planet 105 (E2), 4197–4216.
Jones, J.H., 2003. A liquidus geothermometer for SNC. Lunar and Eucritic magmas. Lunar Planet. Sci. XXXIV. CD-ROM#1130(abs.).

Joy, K.H., Crawford, I.A., Downes, H., Russell, S.S., Kearsley, A.T., 2006. A petrological, mineralogical, and chemical analysis of the lunar mare basalt meteorite LaPaz icefield 02205, 02224, and 02226. Meteorit. Planet. Sci. 41 (7), 1003–1025.
Joy, K., Burgess, R., Hinton, R., Fernandes, V., Crawford, I.A., Kearsley, A., Irving, A., 2011. Petrogenesis and chronology of lunar meteorite Northwest Africa 4472: a KREEPy regolith breccia from the moon. Geochim. Cosmochim. Acta 75 (9), 2420–2452.
Li, Q.L., Zhou, Q., Liu, Y., Xiao, Z., Lin, Y., Li, J.-H., Ma, H.-X., Tang, G.Q., Guo, S., Tang, X., Yuan, J.-Y., Li, J., Wu, F.-Y., Ouyang, Z., Li, C., Li, X.H., 2021. Two-billion-year-old volcanism on the moon from Chang'E-5 basalts. Nature 600 (7887), 54–58.
Li, C., Hu, H., Yang, M.-F., Pei, Z.-Y., Zhou, Q., Ren, X., Liu, B., Liu, D., Zeng, X., Zhang, G., Zhang, H., Liu, J., Wang, Q., Deng, X., Xiao, C., Yao, Y., Xue, D., Zuo, W., Su, Y., Wen, W., Ouyang, Z., 2022. Characteristics of the lunar samples returned by Chang'E-5 mission. Natl. Sci. Rev. https://doi.org/10.1093/nsr/nwab1188.
Lindsley, D.H., 1983. Pyroxene thermometry. Am. Mineral. 68, 477–493.
Lindsley, D.H., Burnham, C.W., 1970. Pyroxferroite: stability and X-ray crystallography of synthetic $Ca_{0.15}Fe_{0.8}SiO_3$ pyroxenoid. Science 168 (3929), 364–367.
Liu, Y., Hu, Z., Gao, S., Günther, D., Xu, J., Gao, C., Chen, H., 2008. In situ analysis of major and trace elements of anhydrous minerals by LA-ICP-MS without applying an internal standard. Chem. Geol. 257 (1–2), 34–43.
Longhi, J., Walker, D., Hays, J.F., 1978. The distribution of Fe and mg between olivine and lunar basaltic liquids. Geochim. Cosmochim. Acta 42 (10), 1545–1558.
Naney, M.T., Crowl, D.M., Papike, J.J., 1976. The Apollo 16 drill core-statistical analysis of glass chemistry and the characterization of a high alumina-silica poor/HASP/ glass. In: Lunar and Planetary Science Conference Proceedings, vol. 7, pp. 155–184.
Neal, C.R., Taylor, L.A., 1992. Petrogenesis of mare basalts: a record of lunar volcanism. Geochim. Cosmochim. Acta 56 (6), 2177–2211.
Neal, C.R., Hacker, M.D., Snyder, G.A., Taylor, L.A., Liu, Y.G., Schmitt, R.A., 1994. Basalt generation at the Apollo 12 site, part 1: new data, classification, and re-evaluation. Meteoritics 29, 334–348.
Neal, C.R., Valenciano, J.L., Che, X., Shi, Y., Liu, D., Tao, L., Joy, K.H., Snape, J.F., Tartèse, R., Head, J., Jolliff, B., Nemchin, A., Norman, M.D., 2022. Crystal size distribution of ilmenite in Chang'e-5 basalt clasts. Lunar Planet. Sci. Conf. 53, 2353.
Niu, Y., Gilmore, T., Mackie, S., Greig, A., Bach, W., 2002. Mineral chemistry, whole-rock compositions, and petrogenesis of Leg176 Gabbros: data and discussion. In: Natland, J.H., Dick, H.J.B., VonHerzen, D.J. Millerand R.P. (Eds.), Chapter 8 of Proceedings of the Ocean Drilling Program, Scientific Results, vol. 176.
Papike, J.J., Ryder, G., Shearer, C.K., 1998. Lunar samples. In: Papike, J.J. (Ed.), Planetary Materials. Mineralogical Society of America, Washington, DC, pp. 5-1–5-234.
Papike, J.J., Fowler, G.W., Adcock, C.T., Shearer, C.K., 1999. Systematics of Ni and co in olivine from planetary melt systems: lunar mare basalts. Am. Mineral. 84 (3), 392–399.
Pernet-Fisher, J.F., Howarth, G.H., Liu, Y., Chen, Y., Taylor, L.A., 2014. Estimating the lunar mantle water budget from phosphates: complications associated with silicate-liquid-immiscibility. Geochim. Cosmochim. Acta 144, 326–341.
Potts, N.J., Tartèse, R., Anand, M., van Westrenen, W., Griffiths, A.A., Barrett, T.J., Franchi, I.A., 2016. Characterization of mesostasis regions in lunar basalts: understanding late-stage melt evolution and its influence on apatite formation. Meteorit. Planet. Sci. 51 (9), 1555–1575.
Putirka, K.D., 2008. Thermometers and barometers for volcanic systems. Rev. Mineral. Geochem. 69 (1), 61–120.
Qian, Y., Xiao, L., Head, J.W., van der Bogert, C.H., Hiesinger, H., Wilson, L., 2021a. Young lunar mare basalts in the Chang'e-5 sample return region, northern Oceanus Procellarum. Earth Planet. Sci. Lett. 555, 116702.
Qian, Y., Xiao, L., Wang, Q., Head, J.W., Yang, R., Kang, Y., van der Bogert, C.H., Hiesinger, H., Lai, X., Wang, G., Pang, Y., Zhang, N., Yuan, Y., He, Q., Huang, J., Zhao, J., Wang, J., Zhao, S., 2021b. China's Chang'e-5 landing site: geology, stratigraphy, and provenance of materials. Earth Planet. Sci. Lett. 561, 116855.
Qian, Y., Xiao, L., Head, J.W., Wöhler, C., Bugiolacchi, R., Wilhelm, T., Althoff, S., Ye, B., He, Q., Yuan, Y., Zhao, S., 2021c. Copernican-aged (<200 Ma) impact ejecta at the Chang'e-5 landing site: statistical evidence from crater morphology, morphometry, and degradation models. Geophys. Res. Lett. 48, e2021GL095341 https://doi.org/10.1029/2021GL095341.
Righter, K., Collins, S.J., Brandon, A.D., 2005. Mineralogy and petrology of the LaPaz icefield lunar mare basaltic meteorites. Meteorit. Planet. Sci. 40 (11), 1703–1722.
Roedder, E., 1978. Silicate liquid immiscibility in magmas and in the system K_2O-FeO-Al_2O_3-SiO_2: an example of serendipity. Geochim. Cosmochim. Acta 42, 1597–1617.
Roedder, E., Weiblen, P.W., 1970. Silicate liquid immiscibility in lunar magmas, evidenced by melt inclusions in lunar rocks. Science 167 (3918), 641–644.
Roedder, E., Weiblen, P.W., 1971. Petrology of silicate melt inclusions, Apollo 11 and Apollo 12 and terrestrial equivalents. Proc. Lunar Sci. Conf. 2nd, 507–528.
Roedder, E., Weiblen, P.W., 1972. Petrographic features and petrologic significance of melt inclusions in Apollo 14 and 15 rocks. Proc. Lunar Sci. Conf. 3rd, 251–279.
Roeder, P.L., Emslie, R., 1970. Olivine-liquid equilibrium. Contrib. Mineral. Petrol. 29 (4), 275–289.
Rutherford, M.J., Hess, P.C., Daniel, G.H., 1974. Experimental liquid line of descent and liquid immiscibility for basalt 70017. In: Lunar and Planetary Science Conference Proceedings, vol. 5, pp. 569–583.
Saal, A.E., Hauri, E.H., Cascio, M.L., Van Orman, J.A., Rutherford, M.C., Cooper, R.F., 2008. Volatile content of lunar volcanic glasses and the presence of water in the Moon's interior. Nature 454 (7201), 192–195. https://doi.org/10.1038/nature07047.
Schwinger, S., Breuer, D., 2022. Employing magma ocean crystallization models to constrain structure and composition of the lunar interior. Phys. Earth Planet. Inter. 322, 106831.
Shaulis, B.J., Righter, M., Lapen, T.J., Jolliff, B.L., Irving, A.J., 2017. 3.1 Ga crystallization age for magnesian and ferroan gabbro lithologies in the Northwest Africa 773 clan of lunar meteorites. Geochim. Cosmochim. Acta 213, 435–456.
Shearer, C.K., Papike, J.J., 1993. Basaltic magmatism on the moon: a perspective from volcanic picritic glass beads. Geochim. Cosmochim. Acta 57 (19), 4785–4812.
Shearer, C.K., Hess, P.C., Wieczorek, M.A., Pritchard, M.E., Parmentier, E.M., Borg, L.E., Wiechert, U., 2006. Thermal and magmatic evolution of the Moon. Rev. Mineral. Geochem. 60 (1), 365–518.
Smith, P.M., Asimow, P.D., 2005. Adiabat_1ph: a new public front-end to the MELTS, pMELTS, and pHMELTS models. Geochem. Geophys. Geosyst. 6 (2).
Stadermann, A.C., Jolliff, B.L., Krawczynski, M.J., Hamilton, C.W., Barnes, J.J., 2022. Analysis and experimental investigation of Apollo sample 12032,366-18, a chemically evolved basalt from the moon. Meteorit. Planet. Sci. https://doi.org/10.1111/maps.13795.
Sun, S.S., McDonough, W.F., 1989. Chemical and isotopic systematics of oceanic basalts: implications for mantle composition and processes. Geol. Soc. Lond., Spec. Publ. 42 (1), 313–345.
Terada, K., Anand, M., Sokol, A.K., Bischoff, A., Sano, Y., 2007. Cryptomare magmatism 4.35 Gyr ago recorded in lunar meteorite Kalahari 009. Nature 450 (7171), 849–852.
Tian, H.C., Wang, H., Chen, Y., Yang, W., Zhou, Q., Zhang, C., Wu, F.Y., 2021. Non-KREEP origin for Chang'e-5 basalts in the Procellarum KREEP terrane. Nature 600 (7887), 59–63.
Warren, P.H., 1988. The origin of pristine KREEP-effects of mixing between UrKREEP and the magmas parental to the mg-rich cumulates. In: Lunar and Planetary Science Conference Proceedings, vol. 18, pp. 233–241.
Warren, P.H., 1989. KREEP: major-element diversity, trace-element uniformity (almost). In: Moon in Transition: Apollo 14, KREEP, and Evolved Lunar Rocks, pp. 149–153.
Webb, S., Neal, C.R., Che, X., Shi, Y., Liu, D., Tao, L., Joy, K.H., Snape, J.F., Tartèse, R., Head, J., Jolliff, B., Nemchin, A., Norman, M.D., 2022. Crystal size distribution of plagioclase in basalt fragments from Oceanus Procellarum recovered by Chang'e-5. Lunar Planet. Sci. Conf. 53, 2896.
Whitten, J.L., Head, J.W., 2015. Lunar cryptomaria: physical characteristics, distribution, and implications for ancient volcanism. Icarus 247, 150–171.
Wieczorek, M.A., Jolliff, B.L., Khan, A., Pritchard, M.E., Weiss, B.P., Williams, J.G., Bussey, B., 2006. The constitution and structure of the lunar interior. Rev. Mineral. Geochem. 60 (1), 221–364.
Wilson, L., Head, J.W., Qian, Y., Xiao, L., 2022. Modelling the eruption of the lavas sampled by the Change'e-5 mission. Lunar Planet. Sci. Conf. 53 abstract #1624.
Zeigler, R., Korotev, R.L., Haskin, L.A., Jolliff, B.L., Gillis, J.J., 2006. Petrography and geochemistry of five new Apollo16 mare basalts and evidence for post-basin deposition of basaltic material at the site Meteorit. Planet. Sci. 41, 263–284.
Zeng, X., Li, X., Liu, J., Mo, B., Yu, W., Tang, H., 2020. Discerning lunar pyroclastic and impact glasses via Raman spectroscopy. J. Geophys. Res. Planet 125, e2020JE006674. https://doi.org/10.1029/2020JE006674.
Zhao, J., Xiao, L., Qiao, L., Glotch, T.D., Huang, Q., 2017. The Mons Rümker volcanic complex of the moon: a candidate landing site for the Chang' E-5 mission. J. Geophys. Res. Planet 122 (7), 1419–1442.
Ziethe, R., Seiferlin, K., Hiesinger, H., 2009. Duration and extent of lunar volcanism: comparison of 3D convection models to mare basalt ages. Planet. Space Sci. 57, 784–796. https://doi.org/10.1016/j.pss.2009.02.002.